Journal of Power Sources 249 (2014) 219–230

Contents lists available at ScienceDirect

Journal of Power Sources

journal homepage: www.elsevier.com/locate/jpowsour

Diffusive relaxation of Li in particles of silicon oxycarbide measured by galvanostatic titrations

P.D. Weidman, Dongjoon Ahn, R. Raj*

Department of Mechanical Engineering, University of Colorado at Boulder, Boulder, CO 80309-0427, USA

HIGHLIGHTS

- We show that diffusive relaxation during galvanostatic titrations embodies one principal time constant.
- The time constant is independent of the rate of injection of Li just prior to the open circuit galvanostatic relaxation.
- The time constant is related explicitly to the particle size and to the chemical diffusivity of Li in the active material.

ARTICLE INFO

Article history:
Received 14 June 2013
Received in revised form
18 September 2013
Accepted 21 September 2013
Available online 2 October 2013

Keywords:
Lithium ion
Batteries
Chemical diffusion
GITT
Silicon-oxycarbide

ABSTRACT

Experiments with silicon-oxycarbide, an anode material for Li-ion batteries, are compared with a rigorous solution for time-dependent diffusion profiles in spherical particles, which is supplemented by finite element analyses of cuboid shaped particles. In this way a value for the chemical diffusivity $D = 1.8 \times 10^{-18}$ -4.2×10^{-18} m^2 s^{-1} across the entire range of the state-of-charge is obtained. The method consists of galvanostatic titrations, where a constant current injection is followed by the measurement of the galvanic potential in open circuit relaxation, at various values of the state-of-charge. Comparison with theory shows that the relaxation time varies with the state-of-charge because the particles have variable size: small particles have short relaxations and dominate the low values of the state-of-charge. The theoretical results have additional notable features. We show that the solution for the spherical particles can be represented to a very good approximation by a single time constant of exponential relaxation. Its value is significantly slower than the results for one-dimensional solutions. The relaxation time is independent of the injection current and the state-of-charge, imparting significant generality to the results.

1. Introduction

The diffusivity of lithium into anode and cathode materials controls the rate at which batteries can be charged and discharged. It is therefore a fundamental parameter for materials-selection in battery design.

The effective rate of Li insertion or extraction is related to the physical length scale of the electrode material, λ, and to the coefficient of chemical diffusion of Li in the host material, which we write as D. From dimensional arguments the typical time for diffusion, t, across this length scale, can be normalized according to the scaling law

$$\lambda^2 = mDt \tag{1}$$

where m is a dimensionless parameter whose value can vary significantly depending on the geometry of the diffusion field. A key objective of the present work is to provide exact descriptions for the diffusion of Li into spherical particles in ways that can be easily compared with experiment in order to elicit values for the chemical diffusivity of Li. The experiments are carried out on silicon-oxycarbide, an anode material for Li-ion batteries.

The architecture of a typical anode is illustrated in Fig. 1 [1]. The anode particles are connected electrically to the current collector via a conducting agent (typically carbon black). The voltage is measured across the half-cell with pure Li metal as the reference electrode. In the open-circuit condition when no current flows through the cell, this voltage is related to the chemical activity of Li on the surface of the particles, a_{Li}, by the Nernst equation

$$V = \frac{RT}{F}\ln(a_{Li}). \tag{2}$$

where F is the Faraday constant. Since activity of lithium in the host must be less than that of pure metal, $a_{Li} \leq 1$, and therefore $V \leq 0$.

* Corresponding author. +1 303 492 1029.
E-mail address: rishi.raj@colorado.edu (R. Raj).

0378-7753/$ – see front matter © 2013 Elsevier B.V. All rights reserved.
http://dx.doi.org/10.1016/j.jpowsour.2013.09.087

Nomenclature

a, r	the radius of the electrode particle, and the radial coordinate from the center of the particle.
$c(r,t)$	the spatial and time-dependent concentration (moles per unit volume) of the diffusing species.
$\bar{c}(t)$	the volume-averaged charge state, i.e. the total charge (in moles) injected into the particle divided by the volume of the particle.
$c_a(t)$, $c_a(\tau)$	concentration at the surface of the particle.
t	real time
τ	dimensionless time
J_0	injection rate written as flux per unit area entering the particle
D_F	Fickian diffusion coefficient
D	chemical diffusion coefficient
t_0, τ_0	period of current injection in real and dimensionless time
t^*, τ^*	real and dimensionless time measured from the start of open circuit relaxation
Δt^*	time constant for the exponential relaxation of surface concentration during open circuit
Q_{Li}	Li capacity in mAh g^{-1}
SOC	the state-of-charge defined as the fraction of the full capacity of the material achieved at a given current density
α	a nondimensional parameter for calculating the relationship between Li concentration and open circuit voltage.
α_V	a modified version of α in units of V.

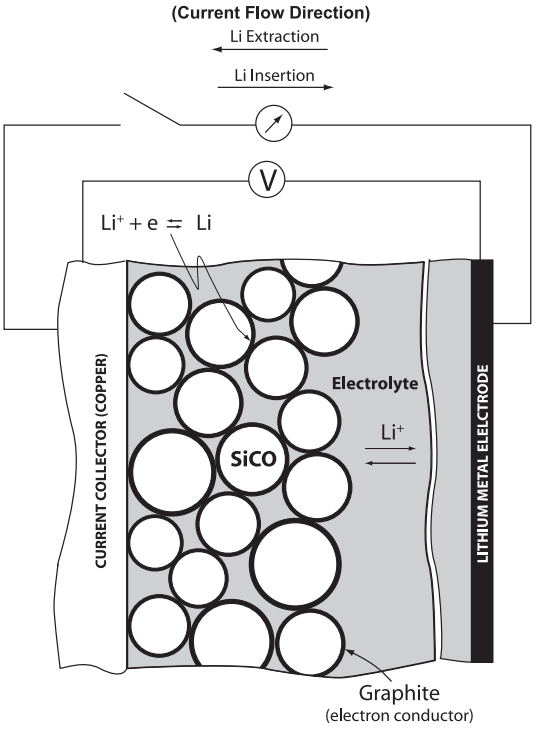

Fig. 1. The architecture of the anode for the Li-ion half-cell in the present experiments. The analysis addresses the diffusion of Li into the silicon-oxycarbide particles.

The relationship between concentration and the activity of Li is discussed in Section 4.

The diffusivity of Li in electrode materials is often measured in one of two ways, known as PITT [2] and GITT [3]. In PITT a step voltage is applied, and the current transient is measured. In GITT a short pulse of current is applied, followed by the measurement of the voltage response in open-circuit. The relaxation time is substituted into an equation having the form given in Eq. (1) for an estimate of the diffusivity. The GITT method is expected to be more reliable for the determination of the relaxation since it avoids errors stemming from interfacial polarizations and resistive potential drops across the electrolyte [4,5].

The theory and experiment presented here are concerned with galvanostatic titrations for particles of spherical geometry and cuboid shapes. The parameters are normalized in order to obtain self-consistent values for the coefficient of chemical diffusion from experiments carried out for different values of injection currents, states-of-charge, and particle size.

The following section begins with the theoretical results, followed by experimental measurements which are then compared with theory.

2. Analysis

The diffusion transport of Li into electrode materials is often analyzed with Fick's first law, where the flux is equal to the product of the diffusion coefficient and the concentration gradient [6]. We call this the Fickian diffusion coefficient, D_F. However, in situations that involve chemical reactions it is more appropriate to consider the gradient of the chemical potential as the driving force for diffusion; in this instance the chemical diffusion coefficient, D, is the measure of diffusivity. The two diffusion coefficients are related by the change in the chemical activity with concentration. In the sequel open-circuit-relaxation measurements are used to determine the value for this factor.

In the next section two specific diffusion problems are solved. First the species (Li) is inserted into the particle at a constant current, and the resulting time-dependent concentration profile of Li in the particle is determined. In the next step, the current is stopped (the open-circuit condition) and the relaxation of the voltage profile with time is analyzed. Subsequently, these results will be used as the basis for interpreting experiments of Li intercalation into particles of silicon-oxycarbide.

2.1. Description of the analysis

The problems solved below are described in Fig. 2. Under constant current, as shown on the left, the surface concentration rises monotonically with time. Under open circuit, shown on the right, the surface concentration decreases with time as the concentration relaxes, eventually reaching a uniform value throughout the particle.

2.1.1. The governing equation

The governing equation for time varying diffusion that enforces mass balance and continuity of concentration in space and time, for a spherical geometry is given by

$$\frac{\mathrm{d}c(r,t)}{\mathrm{d}t} = D_F\left(\frac{\partial^2 c}{\partial r^2} + \frac{2}{r}\frac{\partial c}{\partial r}\right). \tag{3}$$

2.1.2. Normalization of variables

The volume-averaged concentration in the particle is readily obtained as the product of the injection rate into the particle (equal

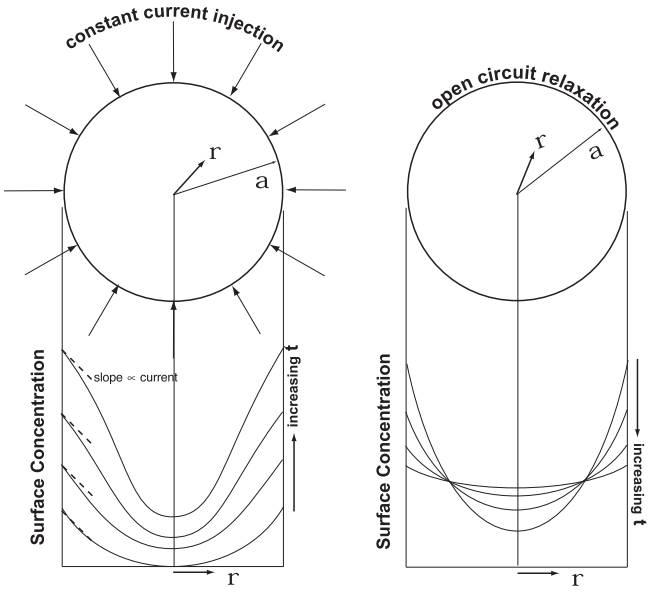

Fig. 2. Schematics of concentration profiles of Li in a particle during insertion at a constant current, followed by diffusional smoothing in open circuit.

to the flux times the particle surface area) multiplied by the duration of injection divided by the volume of the particle. These substitutions lead to

$$\overline{c}(t) = \frac{3J_0}{a}t. \tag{4}$$

The analysis leads, naturally, to normalization of time, τ, given by

$$\tau = \frac{D_F t}{a^2}. \tag{5}$$

The dimensionless radial coordinate is

$$R = \frac{r}{a}. \tag{6}$$

Combining Eqs. (4)–(6) gives the average concentration in terms of normalized time as

$$\overline{c}(t) = \frac{3aJ_0}{D_F}\tau. \tag{7}$$

Note that we analyze the problem in the real-time domain. An alternative approach with Laplace transforms has been used by White and co-workers [6].

2.2. Results for constant current injection

In this problem we seek the change in the surface concentration with time when a constant current is injected into the particle which implies the boundary and initial conditions

$$J_0 = D_F\left.\frac{\partial c(r,t)}{\partial r}\right|_{r=a}, \quad \left.\frac{\partial c(r,t)}{\partial r}\right|_{r=0} = 0, \quad c(r,0) = 0 \tag{8}$$

The first condition specifies that the radial gradient of the concentration at the surface is equal to the injection rate. The second condition arises from the spherical symmetry of the problem, and the last relation ensures that the initial concentration is zero everywhere within the particle.

The solution to the governing equation subject to the boundary conditions specified in Eq. (8) is given in Appendix A. We thereby obtain the concentration at the surface of the particle, expressed in dimensionless time as

$$c_a(\tau) = \frac{3aJ_0}{D_F}\tau + \frac{aJ_0}{D_F}\left(\frac{1}{5} - 2\sum_1^\infty \frac{e^{-\beta_n^2\tau}}{\beta_n^2}\right) \tag{9}$$

where the eigenvalues β_n satisfy

$$\beta_n = \tan\beta_n. \tag{10}$$

In order to understand the behavior predicted by Eq. (9), it is useful to write it in the dimensionless form

$$\frac{c_a(\tau)}{\left(\frac{3aJ_0}{D_F}\right)} = \tau + \frac{1}{3}\left(\frac{1}{5} - 2\sum_1^\infty \frac{e^{-\beta_n^2\tau}}{\beta_n^2}\right). \tag{11}$$

The asymptotic behavior of Eq. (11) as $\tau \to \infty$ is given by

$$\frac{c_a(\tau)}{\left(\frac{3aJ_0}{D_F}\right)} \sim \tau + \frac{1}{15} \quad \text{as} \quad \tau \to \infty. \tag{12}$$

The surface concentration increases linearly with time at large time, with 1/15 intercept on the ordinate.

A reasonable approximation to Eq. (11) is obtained by expanding the sum and considering only the first term. The first three eigenvalues are $\beta_1 = 4.5$, $\beta_2 = 7.7$, and $\beta_3 = 10.9$. Since terms in the expansion decay exponentially with β_n^2, only the first term would make a significant contribution leading to the result

$$\frac{c_a(\tau)}{\left(\frac{3aJ_0}{D_F}\right)} \simeq \tau + \frac{1}{15}\left(1 - \frac{1}{2}e^{-20\tau}\right). \tag{13}$$

The exact result from Eq. (11), with the asymptotic override, is shown in Fig. 3. The plots show two regimes of behavior: the transient regime, which has duration of $\tau = 0.05$, followed by a steady state regime. The transient, which we call Δt_J, with the subscript standing for the constant current case, is related to the diffusion coefficient via Eq. (5)

$$D_F \simeq \frac{0.05a^2}{\Delta t_J}. \tag{14}$$

Plots for Eq. (11) that include only the first term, β_1, two terms β_1, β_2, and three terms β_1, β_2, β_3, are shown in Fig. 3. The result from

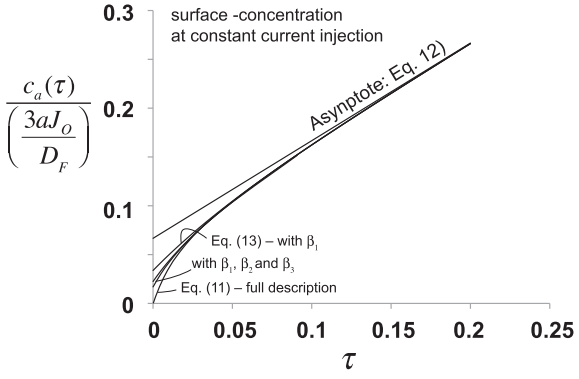

Fig. 3. Plots of Eq. (11) showing the change in surface concentration with time. The full plot, as well as the asymptote and plots for one, two and three terms from the summation of the exponential terms are shown.

Eq. (13), which includes only the first term, gives a very good approximation to the exact result for all $\tau \geq 0.03$.

In the second problem considered below, the current is stopped and the diffusing species are allowed to relax towards a uniform concentration within the particle.

2.3. Analysis for open circuit relaxation

In this section we analyze the problem where the current is stopped at $t = t_0$, and the concentration within the particle is allowed to relax by diffusion, eventually leading to a uniform concentration. This uniform concentration is given by Eq. (4), evaluated at time t_0.

To track the time in the open circuit state, we introduce the new time variable, t^*, defined as

$$t^* = t - t_0 \tag{15}$$

where t^* begins after the current is stopped. The normalized time variables, τ_0 and τ^* are defined in the same way as is τ in Eq. (5).

This problem is solved in Appendix B, with the boundary condition

$$\left.\frac{\partial c(r,t)}{\partial r}\right|_{r=0} = 0 \tag{16}$$

and with the $t^* = 0$ initial condition

$$c(r,0) = \frac{3J_0 t_0}{a} - \frac{3J_0 a}{10D_F} + \frac{J_0 r^2}{2aD_F} - \frac{2J_0 a}{D_F}\sum_1^\infty \frac{\sin(\beta_n R)}{\beta_n^2 R \sin\beta_n} e^{-\beta_n^2 \tau_0} \tag{17}$$

where

$$\tau_0 = \frac{D_F t_0}{a^2} \tag{18}$$

The analysis gives the following evolution of surface concentration with time

$$\frac{c_a(\tau^*)}{\frac{3aJ_0}{D_F}} = \tau_0 + \frac{2}{3}\sum_1^\infty e^{-\beta_n^2\tau^*}\frac{1 - e^{-\beta_n^2\tau_0}}{\beta_n^2} \tag{19}$$

This can be simplified to a very good approximation by considering only the first term in the expansion, *viz.*

$$\frac{c_a(\tau^*)}{\frac{3aJ_0}{D_F}} \simeq \tau_0 + \frac{1}{30}e^{-20\tau^*}\left(1 - e^{-20\tau_0}\right) \tag{20}$$

Eq. (20) has the correct long time limit. That is, when $\tau^* > \tau_0$, the second term on the right hand side vanishes, giving the expected result that the surface concentration becomes equal to the average concentration within the particle as given by Eq. (7).

In order to compare Eq. (20) to experiment, it is useful to write it in the form

$$\frac{30\tau_0}{\bar{c}(\tau_0)\left(1 - e^{-20\tau_0}\right)}\Delta c_a(\tau^*) \simeq e^{-20\tau^*} \tag{21}$$

where

$$\Delta c_a = c_a(\tau^*) - \bar{c}(\tau_0).$$

Eq. (21) specifies that the evolution of the concentration from its initial value, $c_a(\tau^*)$, to its uniform steady state value, $c_a(\tau_0)$, is approximated by an exponential decay, meaning that the concentration falls to $(1/e)$ of its initial value after a period of $20\tau^*$.

The result in Eq. (21) is particularly relevant to experimental measurement. It predicts that the surface concentration will decay exponentially at the same rate regardless of the magnitude and the duration of the current injection.

In the following section the above results are applied to electrochemical data from half-cells where anodes are made from particles of silicon-oxycarbide.

3. Experiments

3.1. The method

The experiments were carried out with electrochemical insertion of Li into anodes made from particles of amorphous silicon-oxycarbide, employing Li metal as the counter electrode. These materials are made by controlled pyrolysis of siloxanes, which are silicon based polymers. They are amorphous. Their structure consists of a stochastic network of graphene, with an average domain size of ~2 nm. The intradomain spaces are filled with SiO_4 tetrahedra, but the interfaces with graphene also contain mixed bond tetrahedra constructed from Si–C–O [7].

The procedure for the preparation of the powders and the assembly of the half cells are described in Ref. [1]. The composition of the amorphous material for the present study was $SiC_{1.98}O_{0.85}$. The average size of the particles in the powder was ~5 μm. The electrode was prepared by mixing SiCO powders with carbon black and a binder into slurry, which was screen printed on a copper foil with a doctor blade, followed by drying and pressing. The thickness of the electrode material on copper produced in this way was 50–70 μm. Lithium foil was used as the counter and reference electrode. The electrodes were sandwiched with microporous polypropylene (Celgard, USA) and filled with the electrolyte consisting of a solution of 1 M LiPF6 and diethyl carbonate (volume ratio 1:1, Ferro Corporation, USA). The coin cells were assembled, crimped and closed in an Argon filled glove box.

The electrochemical measurements were performed at insertion and extraction current density of 50 mA g^{-1} between voltage limits of 0.01 V and ~3 V. The silicon oxycarbide materials show a first cycle loss of ~30% but are stable and reversible in subsequent cycling. Their reversible capacity is 700–1000 mAh g^{-1} at about 0.2 C h^{-1}. These materials can sustain very high C-rates without failure [8].

3.2. Galvanostatic titrations

The results reported here are in the stable and reversible cycling regime. The starting state for the titration experiments consisted of extracting lithium from the anode with a current of 50 mAh g^{-1} until reaching 3 V, at which point the anode was assumed to be essentially depleted of Li.

Current was then injected into the anode (at 50 mAh g^{-1}) for 30 min, equivalent to Li insertion of 25 mA g^{-1}. Next, the current was interrupted and the voltage was measured in open circuit, which gradually rose with time towards a constant value (diffusion relaxes the surface concentration which leads to a higher voltage). The voltage reached a steady state at the end of 24 h; at this point the Li concentration in the particle was assumed to have become uniform. These two steps, current injection followed by open circuit relaxation, constituted one episode in a series of twenty similar episodes repeated successively, with each episode building on the one before. The results are given in Fig. 4. The data are plotted in two ways: the upper graph gives the cell voltage versus time, and the lower versus capacity. In the time domain the current injection portion is short and the relaxation portion for each episode is long. In the capacity domain the vertical segments represent open circuit

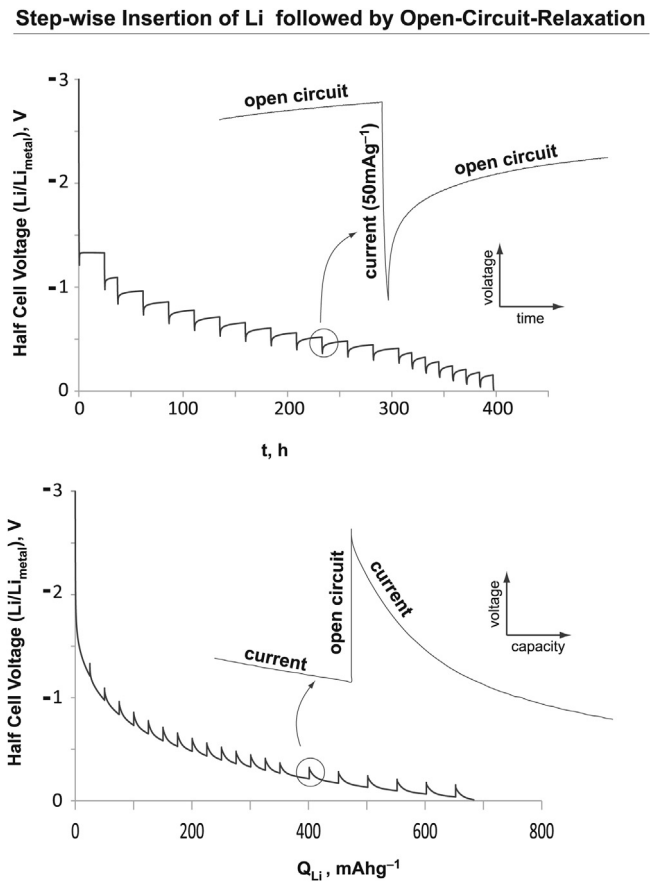

Fig. 4. Twenty steps of current injection followed by relaxation with the cell voltage plotted against time (upper figure), and against the total inserted charge (lower figure). Adopted from Ref. [1].

relaxations (at constant capacity) which are followed by injection of additional Li into the material.

The steady state values of the voltage from each of the open circuit experiments are summarized in Table 1. They list this voltage and the corresponding capacity for each episode. The potential changes form 1.31 V at 25 mA g^{-1} to 0.16 V at 652 mA g^{-1}. The capacities are also expressed as the state-of-charge (SOC) by recognizing that the capacity when charged up to 0.01 V is 1015 mA g^{-1}. The start and end time for the open circuit relaxation for each episode is given in the left columns of Table 1.

Table 1
Steady state Nernst potential measured after open-circuit-relaxation at different levels of the state-of-charge.

Episode#	OCR start	OCR end	Capacity Q_{Li}	Steady state potential	State-of-charge
	h	h	mAh g^{-1}	V	%
1	0.5	24.5	25	1.31	2.2
2	25.0	37.0	50	1.09	4.4
3	37.5	61.5	75	0.96	6.4
4	62.0	86.0	100	0.86	8.6
5	86.5	110.5	125	0.78	10.8
6	111.0	135.0	150	0.69	13.0
7	135.5	159.5	176	0.66	15.3
8	184.5	208.5	201	0.61	17.7
10	209.0	235.0	251	0.52	22.6
11	235.5	257.5	276	0.48	25.3
12	258.0	282.0	301	0.45	28.0
13	282.5	306.5	326	0.41	30.8
14	307.0	319.0	351	0.37	34.8
15	320.0	332.0	401	0.33	39.5
16	333.0	345.0	451	0.28	44.5
17	346.0	358.0	502	0.24	49.9
18	359.0	371.0	552	0.21	55.0
19	372.0	384.0	602	0.18	59.8
20	385.0	397.0	652	0.16	64.2

The time dependent relaxations contain information about the diffusion of Li from the surface towards the center of the particles. In the following section these data are compared with theory to obtain a value of the chemical diffusivity of Li in silicon-oxycarbide.

4. Determination of chemical diffusivity

We seek to apply the theoretical analysis in Section 2 to the titration results reported in Section 3 in order to elicit a value for the coefficient of chemical diffusion. This is a two-step procedure since the analysis is in terms of the concentration, while diffusion is driven by gradients of the chemical potential. The relationship between the chemical potential and the concentration, the first step, is addressed below.

4.1. Relating chemical potential to concentration

The transport equation for chemical diffusion is

$$\boldsymbol{J}_{\mathrm{Li}} = -\frac{Dc_{\mathrm{Li}}}{RT}\boldsymbol{\nabla}\mu_{\mathrm{Li}} \tag{22}$$

Here D is the coefficient of chemical diffusion, c_{Li} is the volumetric concentration of the diffusion species (Li), with units of number per unit volume, whose chemical potential is written in terms of its activity, a_{Li} as

$$\mu_{\mathrm{Li}} = \mu^0_{\mathrm{Li}} + RT\ln(a_{\mathrm{Li}}). \tag{23}$$

Here the standard state is pure Li metal with an activity of unity and a chemical potential of μ^0_{Li}.

The theoretical analysis in Section 2 has been solved for Fickian diffusion where the flux is proportional to the gradient of the concentration (in units of number of species per unit volume), so that

$$\boldsymbol{J}_{\mathrm{Li}} = -D_{\mathrm{F}}\boldsymbol{\nabla}_{\mathrm{Li}} \tag{24}$$

where D_{F} is the Fickian diffusion coefficient of lithium in the electrode material.

Taking the gradient of Eq. (23), substituting into Eq. (22), and then equating the result to Eq. (24) gives the desired relation between D and D_{F}, namely

$$D_{\mathrm{F}} = \alpha D \tag{25}$$

where

$$\alpha = \frac{\mathrm{d}\ln(a_{\mathrm{Li}})}{\mathrm{d}\ln(c_{\mathrm{Li}})}. \tag{26}$$

Furthermore, combining Eq. (26) with Eq. (2) leads to

$$\alpha = \frac{F}{RT}\,\alpha_v, \quad \text{and} \quad \alpha_v = \frac{\mathrm{d}V}{\mathrm{d}\ln c_{\mathrm{Li}}}. \tag{27}$$

The results of the titration experiments given in Table 1 provide data for the voltage as a function of concentration which can be used to obtain the value for α_{V}.

It is of note that Eq. (27) may be used to calculate the concentration from the measurement of the voltage

$$\frac{c_{Li}}{c_{Li}^0} = e^{V/\alpha_F} \tag{28}$$

where c_{Li}^0 is the maximum charge held by the anode when $V \to 0$.

One still needs a relationship between capacity, measured in units of mA g^{-1}, and c_{Li}. This relation becomes redundant because Eq. (27) is written in terms of the derivative of a logarithm, which is a dimensionless quantity evident from

$$\mathrm{dln}c_{Li} = \frac{dc_{Li}}{c_{Li}}. \tag{29}$$

We denote the capacity as Q_{Li} with units mA g^{-1}. Since the concentration is also the capacity in different units, c_{Li} can be replaced by Q_{Li} to obtain

$$\alpha_V = \frac{dV}{\mathrm{dln}\, Q_{Li}}. \tag{30}$$

Thus the experimental value for α_V can be determined from the slope of a plot of V versus ln Q_{Li}. Such a plot of the data given in Table 1 is shown in Fig. 5. The data fit a straight line whose slope gives $\alpha_V = 0.35$ V. Substituting this value into Eq. (27) gives $\alpha = 13.5$.

A constant value for α, arising from a straight line fit to the data through the full range of capacity, gives a linear proportionality between the Fickian and the chemical diffusion coefficients, which greatly simplifies the application of the analysis to the experiment. The linear fit is ascribed to the amorphous nature of the silicon-oxycarbides and the absence of phase change with Li capacity. The case of systems that encounter phase change is discussed in Section 6.

The next step is to match the time dependent relaxation of the voltage under open-circuit to Eq. (21) in order to extract a value of the time constant Δt^*, in real time which then gives the value for D_F.

4.2. Diffusion during open circuit relaxations

During open circuit relaxation Li diffuses within the particle toward its terminal uniform concentration. Theoretically, the relaxation is given by Eq. (21). The left hand side in this equation is the difference between the surface concentration at time t^* and the steady state concentration achieved after full relaxation. The additional factor $30\tau_0/\bar{c}(\tau_0)(1 - e^{-20\tau_0})$ on the left is a constant that depends on the magnitude and duration of current injection, τ_0; it is independent of time and therefore does not affect the measurement of the time constant for relaxation.

The problem is now well posed since the time dependent concentration can be deduced from the measurement of the voltage

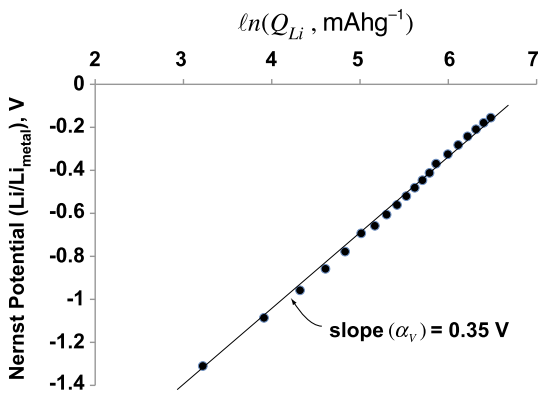

Fig. 5. Plot of data according to Eq. (27) for the determination of α_V.

Table 2
Analysis of the open circuit relaxation data for one episode to obtain the relaxation time which is then matched to experiment as illustrated in Fig. 7.

Relative time for OCR, t^*	Measured cell voltage	Concentration (arb. u.)	Relative concentration	Percent relative concentration
h	V	$\exp(V/\alpha_v)$	Δc_a	$\Delta c_a/0.002993 \times 100$
0.00	−1.2912	0.024993	0.002993	100.0
0.02	−1.2963	0.024632	0.002632	87.9
0.12	−1.3075	0.023856	0.001856	62.0
0.22	−1.3134	0.023457	0.001457	48.7
0.32	−1.3169	0.023224	0.001224	40.9
0.46	−1.3202	0.023006	0.001006	33.6
0.62	−1.3225	0.022855	0.000855	28.6
0.86	−1.3248	0.022706	0.000706	23.6
1.12	−1.3263	0.022609	0.000609	20.3
1.39	−1.3278	0.022512	0.000512	17.1
1.69	−1.3286	0.022460	0.000460	15.4
1.99	−1.3291	0.022428	0.000428	14.3
2.39	−1.3301	0.022364	0.000364	12.2
2.82	−1.3306	0.022332	0.000332	11.1
3.19	−1.3311	0.022301	0.000301	10.0
3.56	−1.3312	0.022294	0.000294	9.8
3.89	−1.3314	0.022281	0.000281	9.4
4.29	−1.3316	0.022269	0.000269	9.0
4.69	−1.3317	0.022262	0.000262	8.8
5.09	−1.3317	0.022262	0.000262	8.8
Steady state after 24 h				
24.0	−1.3358	0.022003	0.000003	0.1

during the relaxation. The relaxation data were matched to Eq. (21) for each of the twenty episodes at different values of the state-of-charge. The method is outlined in Table 2 using one episode as an example. The first column contains the (real) time from the start of the open-circuit experiment. The second column gives the value of the measured cell voltage. The third column converts the voltage to the dimensionless concentration relative to the steady state value obtained after 24 h, which is given at the bottom of the table. The last column reduces the concentration to a fractional value starting with 100% at time zero and approaching zero after 24 h.

The next step is to match the time dependent decay in concentration given in Table 2 to Eq. (21). The procedure is shown in Fig. 6. The main graph shows the time dependent decay in concentration from the right hand columns in Table 2. The objective is

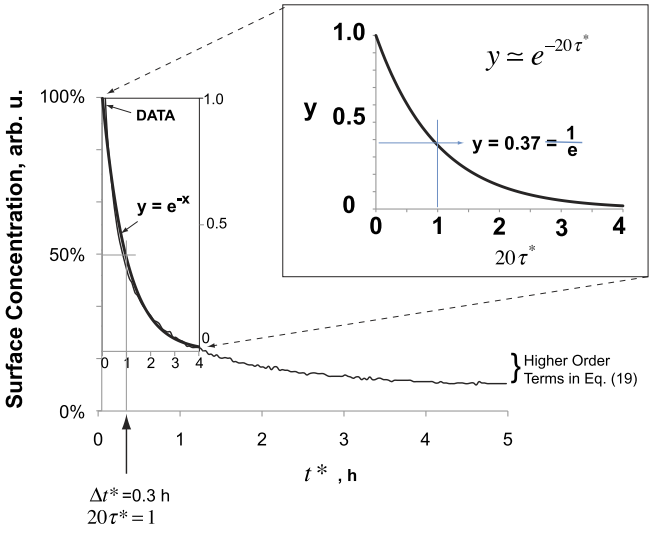

Fig. 6. Procedure for determination of the relaxation time constant by fitting a single exponential term to the data as shown in the inset.

to match this graph to Eq. (21). The left hand side of Eq. (21) is dimensionless. It represents the change in concentration from 100% at $\tau^* = 0$ to zero as $\tau^* \to \infty$. We give it the simpler form

$$y \simeq e^{-20\tau^*} \tag{31}$$

where y represents the dimensionless value of the surface concentration. Eq. (31) is plotted in the inset of Fig. 6. When overlaid on the main graph it provides the equivalence between the dimensionless and real time. The equivalence between the dimensionless time constant $20\tau^*$, and the real time constant Δt^*, is now self evident. Thus when $20\tau^* = 1$, the real time is equal to $\Delta t^* = 0.3$ h.

The definition of normalized time given in Eq. (5) leads to the diffusion coefficient by rewriting it in the form

$$20\tau^* = 20\frac{D_F \Delta t^*}{a^2} = 1 \tag{32}$$

giving

$$D_F = \frac{a^2}{20\Delta t^*} \tag{33}$$

where for the episode illustrated in Fig. 6, $\Delta t^* = 0.3$ h. Substituting this value and the particle size into Eq. (33) gives the value for D_F.

Each of the twenty relaxations were analyzed using the procedure outlined above. They cover a wide range of the state-of-charge (SOC), from 2.2% to 64.2%. These results are shown together in Fig. 7. Remarkably, all relaxations ranging form 4.4%–64.2% SOC fall within a relatively narrow band of $\Delta t^* = 1.5 - 3.5$ h. Considering that the SOC changes by more than a factor of 10, this result reflects good support for the main result of the analysis: the relaxation can be expected to be independent of the duration and extent of the charge injection into the electrode particles.

For the case of SOC = 4.4%–64.2%, we assume a particle radius $a \sim 2.5$ μm. Substituting $\Delta t^* = 1.5 - 3.5$ h into Eq. (33) gives $D_F = 2.5 \times 10^{-17}$–$5.8 \times 10^{-17}$ m^2 s^{-1}. Further substitution into Eq. (25), $\alpha = 13.5$, gives the following value for the chemical diffusion coefficient of Li in silicon-oxycarbide

$$D = 1.8 \times 10^{-18}\text{–}4.2 \times 10^{-18} \text{ m}^2 \text{ s}^{-1} \tag{34}$$

The value in Eq. (34) is lower than the values for diffusion of Li in graphitic structures reported in the literature, which range from 10^{-15} to 10^{-10} m^2 s^{-1} [9]. It is not clear if this difference is actual, or whether it can be attributed to the different ways in which the diffusion coefficients have been measured. The wide variability in the data for graphite in the literature may reflect uncertainties in the measurement methods. The narrow band for the diffusion coefficient measured over a wide range of the state-of-charge is a notable feature of the present work.

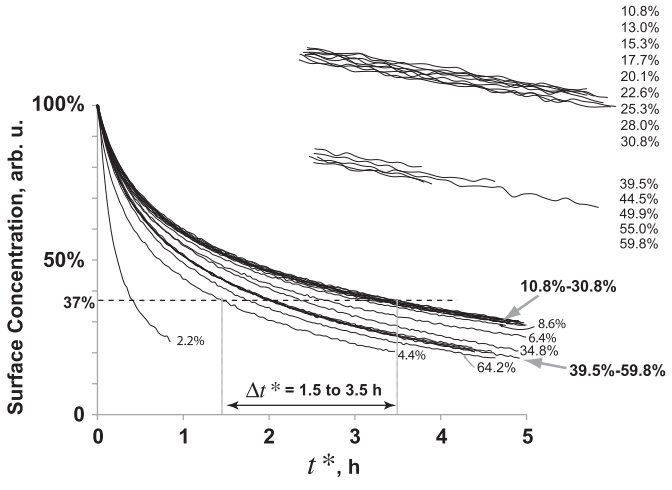

Fig. 7. Plots of surface concentrations in real time for all 20 episodes of open-circuit relaxations. Each plot followed the procedure outlined in Table 2.

4.3. The influence of particle size

In Eq. (33) the diffusion coefficient is a material parameter. Therefore the time constant for relaxation, Δt^*, is related to the particle radius, a. We note in Fig. 7 that the time constant for relaxation is quicker, about 0.3 h for SOC = 2.2%. This is readily explained by the early saturation of small particles in the powder. It can be inferred that the 2.2% of the SOC is held by these particles. It follows that the volume fraction of these small particles in the powder was also about 2.2%. A scanning electron micrograph of the silicon-oxycarbide powder is given in Fig. 8. Note that while most particles have a radius of approximately 5 μm, there is a sprinkling of particles that are much smaller, which we hold responsible for the short relaxation time.

4.4. Analysis of current injection data

The plots in Fig. 3 describe the results for the change in surface concentration as the current is injected into spherical particles at a constant rate. The injection time is prescribed by τ, a normalized parameter, which is related to real time via

$$\tau = \frac{t}{20\Delta t^*}. \tag{35}$$

The above equation is obtained by combining Eq. (5) with Eq. (33). Here t is real time, and Δt^* is measured from the open-circuit-relaxation experiments.

It now becomes possible to compare the change in the surface concentration during current injection, as predicted in Fig. 3, with experiment. This comparison, for episode one, is shown in Fig. 9. Here the time axes for theory and experiment have been synchronized by setting $\Delta t^* = 0.3$ h, the value measured for episode one. For example, $\tau = 0.08$ in dimensionless time is equivalent to 0.5 h in real time. The vertical axis has arbitrary units. The result in Fig. 9 suggests that the solid-electrolyte-interface and the ionic resistance of the electrolyte do not significantly affect the measured cell voltage for the silicon-oxycarbide materials when the current density is 50 mAh g^{-1}. This may not necessarily be the case at higher current densities.

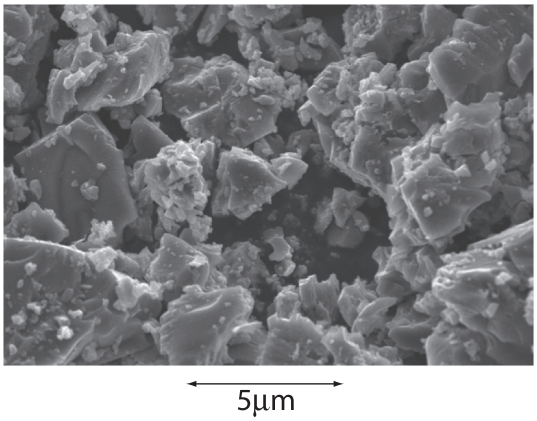

Fig. 8. Scanning electron micrograph of silicon-oxycarbide particles.

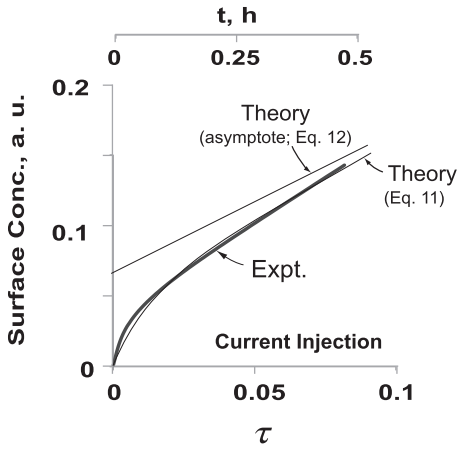

Fig. 9. Comparison of experiment and theory for the change in surface concentration during current injection. The normalized time and real time have been synchronized along the abscissa.

5. Discussion

In this section we compare the present results to similar work in the literature. They are summarized below. The current analysis and experiments are concerned with galvanostatic titrations where intermittent injection of charge at constant rate is followed by measurement of the time dependent relaxation of the galvanic potential at open circuit.

(i) Effect of particle size

According to Eq. (33) the diffusion coefficient is related to both the relaxation time and the particle radius. While the scaling in this result is consistent with Eq. (1), it differs from it by a large numerical factor. The measurements of the relaxation time, Δt^*, as a function of the state-of-charge given in Fig. 7 highlight how its value can vary because small particles become "saturated" with Li quickly. (The small particles normally occupy minor volume fractions since volume is proportional to the third power of particle size.) This result is significant for understanding how the particle size distribution can affect the C-rate capability of electrode materials.

(ii) The three-dimensional nature of the problem

The conventional method for deriving the diffusion coefficient from time dependent relaxations has been to consider one-dimensional diffusion in a semi-infinite slab [3–5], which gives solutions in the form of error functions [10]. Here an exact solution for the three-dimensional problem is presented, and it is rigorously shown that the relaxation time, to a very good approximation, can be described by a single exponential, given by Eq. (31).

The spherical geometry has also been considered in recent work [6,11] where the time dependent problem is approached, not in the real-time, but in the Laplace transform domain. In this approach it is more difficult to extract non-dimensional parameters which can be unambiguously and critically related to experiments. The comparison between theory and experiment in Figs. 6, 7 and 9, are examples of the real-time approach: in these graphs only the time constants for relaxation are needed since the concentrations can be allowed to have arbitrary units.

(iii) Achieving convergence between theory and experiment

We have assiduously sought analytical results that can be applied to experiments, by employing non-dimensional parameters. For example it is noteworthy that the relaxation, given by the right hand side of Eq. (21), is independent of the state-of-charge, and also independent of the rate of insertion of the charge. The only condition is that the relaxation be measured from the moment that the current stops and the open-circuit condition begins. This is a significant simplification in the application of the analysis to experiment. Thus, the usual caveat that the current must be injected very quickly in the GITT method is not necessary.

(iv) Experimental determination of chemical activity as a function of concentration

In order to compare theory with experiment, it is necessary to convert the cell voltage into Li concentration, which requires knowledge of α_V, which is defined in Eq. (30). Its value is obtained by plotting the logarithm of the state-of-charge against the saturation value of Nernst voltage measured in open circuit. Caution must be exercised if α_V can change should the material undergo phase transition. This point is discussed further in the next section.

6. The nuances of theory and experiment

Engineering materials, and the systems that employ them, are nearly always complex. For example, the performance of anodes in a cell depends on the morphology and microstructure of the active material, the architecture of the electrode, and the various kinetic and interfacial reactions.

Efforts to model such engineering systems often follow two approaches. One is to employ numerical, computational methods that seek to simulate the full complexity of the system. The objective of these simulations is to calculate the numerical values of the experimental outcomes. These simulations often do not provide simple parametric relationships between material parameters and cell performance.

In the second approach the phenomenological information from experiments is distilled into concepts that are developed into analytical models. The objective of these closed-form models is to relate the microstructural parameters to experiment. The models build upon fundamental relationships from basic science. While these comparisons require approximations, they serve to provide scaling relationships between microstructure and experimental variables. The deviation of experiment from theory can provide new insights into atomistic mechanisms. In other words this approach enables transparency between science and engineering.

The closed form models necessarily require idealized geometries. For example, the actual shape of the particles, shown in Fig. 8 is clearly not spherical as has been assumed. These assumptions require a nuanced approach to comparing theory with experiment, which we discuss below.

We address three issues: (i) the cuboid shape of the particles as in Fig. 8, (ii) the influence of phase transitions when Li is inserted into an anode material, and (iii) the separation of the time constants during relaxation to determine which one is most likely to be related to the diffusion of Li into the volume of the anode material.

The error from the shape of the particles is addressed by establishing the extent to which the shape deviates from spherical. Exact results for sphere and cuboid shapes, obtained by FEM provide an estimate of this error. An optical micrograph of the particles taken in a cross-sectional view is given in Fig. 10. The particles are angular and look approximately like cuboids with an aspect

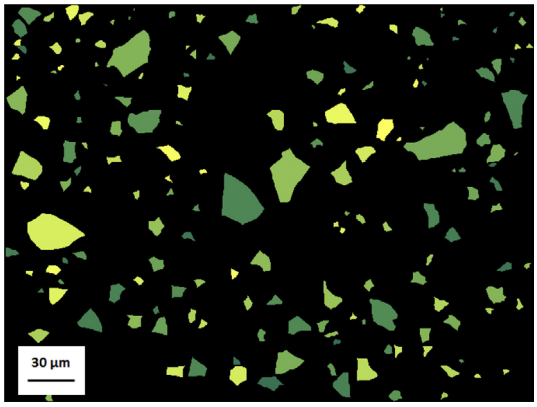

Fig. 10. Optical micrograph of a cross-sectional view of silicone oxycarbide particles.

ratio (the smallest to the largest dimension) in the range of about 0.5–0.75.

Exact results for sphere and cuboid shapes, obtained by finite-element-analysis (FEM) provide an estimate to this error. To determine the extent to which the results for the sphere would be representative for these shapes, we have carried out numerical FEM analysis to determine the time for surface concentration to reach the interior of the particle. The results for a cuboid with an aspect ratio of 0.5, a cube, with an aspect ratio of 1.0, and a sphere all with the same width are shown in Fig. 11. In each case a concentration of unity was applied to the surface as a step function, and the time-dependent concentration at the center of the body was calculated. The cube is approximately two times slower to reach the same concentration at its center than the sphere. The sphere and the cuboid are very similar. The micrograph in Fig. 10 shows that most of the particles have an aspect ratio of approximately 0.5. The inference is that the sphere was quite a good approximation for the diffusion analysis. Even assuming the shapes to be cubes would lead to an error of no more than a factor of two for the diffusion coefficient.

The coefficient of chemical diffusion, D, is proportional to the Fickian diffusion coefficient, D_F, through α, as given in Eq. (25). Experiments with silicon-oxycarbide (SiCO) have shown that α has a constant value. This is perhaps a special case since SiCO is

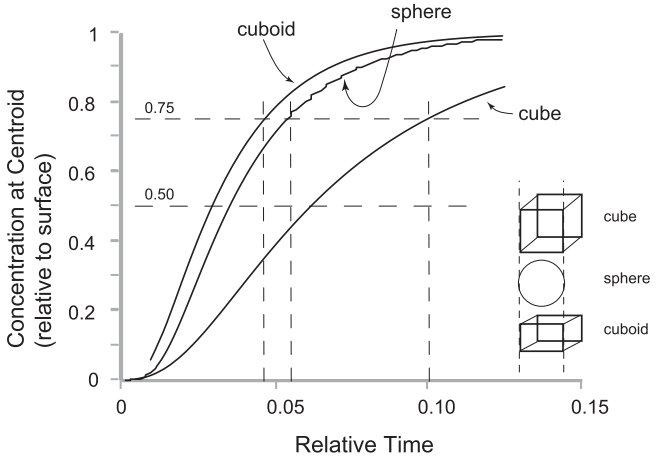

Fig. 11. Plots of the concentration at the core of three particle shapes with time, after the step-function application of unit concentrations at the surface at time zero. The results were obtained from numerical finite element analysis. Note that the cuboid with an aspect ratio of 0.5 behaves similarly to the sphere. The perfect cube is slower by a factor of about two.

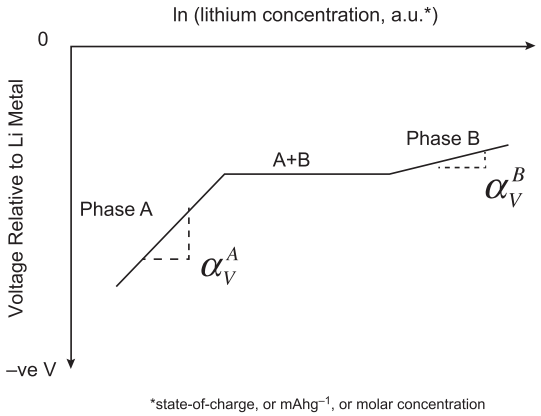

Fig. 12. Conceptual plots of Eq. (A7) in a crystalline material A which transforms to a new phase B when Li is inserted into it. Distinct slopes for α_V can be determined only in the single phase regimes.

amorphous and remains so over the full range of the state of charge. Crystalline materials, however, often encounter a phase transition with Li concentration. Let us say these phases are A and B, with the first being stable at low and the second at high Li concentrations. However, there would also be a range where both phases exist in equilibrium with Li partitioned between them as required by thermodynamic equilibrium. In this two-phase region, Li is expected to partition increasingly to the second phase at the expense of the first, at constant voltage. In this two-phase region the diffusion of Li will be complex. Experimental plots of the type shown in Fig. 12 may be used to identify the single phase regions, and the values for α_V^A and α_V^B for each phase determined from the slopes in the single phase regions.

The third question pertains to the irreversible capacity often seen in the first cycle. The experiments and the theory in this article refer to reversible insertion of lithium, with nearly full coulombic efficiency. The irreversible capacity is sequestered into deep energy levels where it can be assumed to be immobile under the nominal range of voltage levels. One of the key results from the theoretical analysis, which is borne out by experiments, is that the relaxation profile is independent of the prior history of current injection. Furthermore, the relaxation time is independent of the rate and the time period of current injection. The only condition is that the Li concentration in the particle be uniform before current injection. This feature of the results lends considerable generality to the galvanostatic titrations.

Finally, we consider the possible role of extraneous relaxations on the measurement of the diffusion. Equilibration of Li^+ within the electrolyte, and charge transfer at anode–electrolyte interfaces are two examples of such effects. Fortunately, each effect has its own time constant for relaxation. We do see very short relaxations at the onset of the open circuit relaxation. They have negligibly small voltage amplitudes. The time constants for these extraneous relaxations are typically less than 1 min. By comparison, the Li diffusion time constants approach an hour. In our experiments the effect of the extraneous relaxations has been filtered out by taking data 5 min after initiating the open circuit. Further support for the diffusive relaxations lie in their exponential behavior, implying a single mechanism. The systematic and large voltage amplitude of the relaxations further underpins the interpretation of Li diffusion within the particles.

7. Summary

1. Open circuit relaxations, following stepwise injections of Li currents into spherical particles are analyzed. The relaxations

can be described by Eq. (21) which reduces to Eq. (31) for application to data. Thus, the measurements for different levels of injection rate, and state-of-charge, can be represented in a universal curve. That the relaxation time constants are independent of the rate of current injection and the state of charge imparts great generality and simplicity to the galvanostatic titration experiments. In the past it has been assumed that for these experiments to be valid the current must be injected in a short pulse. We show that this condition is unnecessary.
2. Steady state Nernst potentials measured at different states of charge are plotted according to Eq. (27) to obtain a value for α_V. Then, Eq. (28) can be used to convert the voltage into concentration at particle surfaces during open circuit relaxations.
3. The relaxation time Δt^* is related to the Fickian diffusion coefficient through Eq. (33).
4. A distribution in the particle size can produce a spread in the relaxation time. The small particles, which would have a shorter relaxation time, can saturate at low values of the state-of-charge. Therefore the relaxation time can increase with increasing state-of-charge if the particles have a broad size distribution.
5. The change in the surface concentration of the spherical particles during charge injection is analyzed. This result is given in Eq. (11). A comparison of experiment with this analysis provides insight into the significance of interfacial polarization and resistive potential drops across the electrolyte.

Acknowledgments

This research was supported by the Ceramics Program of the Division of Materials Research at the National Science Foundation, under Grant No: DMR-0907108. We wish to thank Kalvis Terauds for the micrograph given in Fig. 10, and Ayazur Rehman for the FEM results presented in Fig. 11. Both are graduate students in Mechanical Engineering at the University of Colorado.

Appendix A. Constant current solution

1 Introduction

In this regime for which $0 \le t \le t_0$ the current flows from the anode to the cathode resulting in a flux J_0 of lithium ions into the sphere. Here one must solve the axisymmetric diffusion equation in spherical coordinates, *viz.*

$$\frac{\partial c}{\partial t} = D_F\left(\frac{\partial^2 c}{\partial r^2} + \frac{2}{r}\frac{\partial c}{\partial r}\right). \tag{A1}$$

The constant flux of ions through the surface of the sphere and the initial concentration of ions being zero lead to the initial and boundary conditions

$$c(r,0) = 0, \quad \left.\frac{\partial c(r,t)}{\partial r}\right|_{r=0} = 0, \quad \left.\frac{\partial c(r,t)}{\partial r}\right|_{r=a} = \frac{J_0}{D_F}. \tag{A2}$$

Since flux is continuously added over time, the sphere continuously increases in ion concentration without bound. This is shown in the following section.

1.1 Volume averaged concentration

We integrate conservation Eq. (A1) over the volume to obtain

$$\int_V \frac{\partial c}{\partial t} dV = D_F \int_V \frac{1}{r^2}\frac{\partial}{\partial r}\left(r^2\frac{\partial c}{\partial r}\right) dV \tag{A3}$$

which gives

$$\frac{\partial}{\partial t}\int_0^a c(r,t) r^2 dr = a^2 J_0. \tag{A4}$$

Integrating on time we find

$$\int_0^a c(r,t) r^2 dr = a^2 J_0 t. \tag{A5}$$

The volume-averaged concentration is defined as

$$\overline{c} = \frac{1}{V}\int_V c(r,t) dV = \frac{3}{a^3}\int_0^a c(r,t) r^2 dr \tag{A6}$$

so that the volume-averaged concentration grows linearly in time, *viz.*

$$\overline{c} = \frac{a^2 J_0 t}{a^3/3} = \frac{3J_0}{a} t. \tag{A7}$$

1.2 Transient solution

Inserting (A7) into (A1) shows that the transient solution will have a term depending on r, thus we write

$$c(r,t) = \overline{c}(t) + F(r) + v(r,t). \tag{A8}$$

into the diffusion equation gives

$$F(r) = \frac{J_0}{2aD_F} r^2 \tag{A9}$$

and the boundary-value problem for $v(r,t)$ becomes

$$\frac{\partial v}{\partial t} = D_F\left(\frac{\partial^2 v}{\partial r^2} + \frac{2}{r}\frac{\partial v}{\partial r}\right) \tag{A10a}$$

$$v(r,0) = -\frac{J_0}{2aD_F} r^2, \quad \left.\frac{\partial v(r,t)}{\partial r}\right|_{r=0} = 0, \quad \left.\frac{\partial v(r,t)}{\partial r}\right|_{r=a} = 0. \tag{A10b}$$

Now the problem is an initial distribution of concentration with zero flux through the sphere. To solve this we transform according to

$$w(r,t) = r v(r,t) \tag{A11}$$

to obtain

$$\frac{\partial w}{\partial t} = D_F \frac{\partial^2 w}{\partial r^2} \tag{A12a}$$

$$w(r,0) = -\frac{J_0}{2aD_F} r^3 \quad w(0,t) = 0, \quad \left.\frac{\partial w(r,t)}{\partial r}\right|_{r=a} = \frac{1}{a} w(a,t). \tag{A12b}$$

The Robin boundary condition causes no problem because it is homogeneous and we therefore have homogeneous boundary conditions with an initial distribution of 'concentration' in these variables. Assuming the separable solution

$$w(r,t) = F(r)G(t) \tag{A13}$$

we find

$$F'' + \frac{\lambda}{D_F}F = 0, \quad F(0) = 0, \quad F'(a) = \frac{1}{a}F(a) \tag{A14}$$

and

$$G' + \lambda G = 0, \quad G(0) = 1 \tag{A15}$$

where λ is the separation constant and primes denote differentiation with respect to the arguments of F and G. The solutions satisfying $F(0) = 0$ and $G(0) = 1$ are

$$F(r) = \sin \alpha_n r, \quad G(t) = e^{-D_F \alpha_n^2 t} \tag{A16}$$

where the separation constant has been set to $\lambda = D_F\alpha_n^2$. Satisfying the Robin boundary condition in (A14) gives the eigenvalue equation

$$\beta_n = \tan \beta_n \tag{A17}$$

where $\beta_n = a\alpha_n$. Inspection of Eq. (A17) shows that there is an additional eigenfunction at $\lambda = 0$ given by $F(r) = r$ so we summarize the eigenfunctions as follows

$$\phi_0(r) = r, \quad (n = 0) \tag{A18a}$$

$$\phi_n(r) = \sin \alpha_n r, \quad (n \geq 1). \tag{A18b}$$

Application of standard Fourier analysis gives the solution

$$w(r,t) = \sum_0^\infty C_n \phi_n(r) e^{-D_F \alpha_n^2 t}. \tag{A19}$$

To satisfy the initial condition we must have

$$w(r,0) = \sum_0^\infty C_n \phi_n(r) = -\frac{J_0}{2aD_F} r^3 \tag{A20}$$

for which the constants C_0 and C_n for $(n \geq 1)$ are readily found to be

$$C_0 = -\frac{3}{10}\frac{J_0 a}{D_F}, \quad C_n = -\frac{2J_0}{D_F \alpha_n^2 \sin(a\alpha_n)}. \tag{A21}$$

Use of eigenvalue Eq. (A18) has been made to obtain the simplified form for C_n given above. Now the solution for $w(r,t)$ is

$$w(r,t) = -\frac{3}{10}\frac{J_0 a}{D_F} r + \sum_1^\infty C_n \sin(\alpha_n r) e^{-D_F \alpha_n^2 t} \tag{A22}$$

and thus

$$v(r,t) = -\frac{3}{10}\frac{J_0 a}{D_F} + \frac{1}{r}\sum_1^\infty C_n \sin(\alpha_n r) e^{-D_F \alpha_n^2 t}. \tag{A23}$$

Finally, from Eq. (A8) we obtain, on reversion to β_n, the final solution

$$c(r,t) = \frac{3J_0}{a}t + \frac{J_0(5r^2 - 3a^2)}{10aD_F} - \frac{2J_0 a^2}{D_F}\frac{1}{r}\sum_1^\infty \frac{\sin(\beta_n r/a) e^{-D_F \beta_n^2 t/a^2}}{\beta_n^2 \sin \beta_n} \tag{A24}$$

In terms of dimensionless radius $R = r/a$ and time $\tau = D_F t/a^2$ we have

$$\frac{c(R,\tau)}{aJ_0/D_F} - 3\tau = \frac{1}{10}\left(5R^2 - 3\right) - \frac{2}{R}\sum_1^\infty \frac{\sin(\beta_n R) e^{-\beta_n^2 \tau}}{\beta_n^2 \sin \beta_n} \tag{A25}$$

The normalized surface values can be easily computed as function dimensionless time τ by evaluating (A25) at $R = 1$ which gives

$$\frac{c(1,\tau)}{aJ_0/D_F} - 3\tau = \frac{1}{5} - 2\sum_1^\infty \frac{e^{-\beta_n^2 \tau}}{\beta_n^2}. \tag{A26}$$

Appendix B. Open circuit relaxation

1 Introduction

In this case the ion current to the sphere stops at $t = t_0$, and the concentration gradient within the sphere relaxes by diffusion to a final uniform concentration. Being interested now in times greater than t_0 we introduce the new time variable $t^* = t - t_0$.

1.1 Final steady state

Before determining the time-dependent adjustment to the final uniform concentration we compute the final steady-state, volume-averaged concentration. To this end one simply evaluates (A24) at $t = t_0$ and then computes the volume averaged concentration as

$$\overline{u}(t \to \infty) = \frac{1}{V}\int_V u(r,t_0)\mathrm{d}V \tag{B1}$$

In performing the integration it is found that contributions from the r-dependent terms in (A24) are zero, so the only contribution is from the first term which gives the final equilibrated concentration as

$$\overline{u}(t \to \infty) = \frac{3J_0 t_0}{a}. \tag{B2}$$

1.2 Adjustment to final steady state

We now solve the diffusion equation given (A1) with no flux at the sphere wall and with the known distribution of concentration calculated from (A24) at the stopping time $t = t_0$ for which $t^* = 0$. Thus the boundary conditions for (A1) are

$$c(a,t^*) = 0, \quad \left.\frac{\partial c(r,0)}{\partial r}\right|_{r=a} = 0,$$
$$c(r,0) = f(r) \equiv A + Br^2 - \sum_{m=1}^\infty P_m \frac{\sin(\alpha_n r)}{r} \tag{B3a}$$

where

$$A = \frac{3J_0 t_0}{a} - \frac{3J_0 a}{10D_F}, \quad B = \frac{J_0}{2aD_F}, \quad P_m = \frac{2J_0 a^2}{D_F \beta_m^2 \sin \beta_m} e^{-D_F \beta_m^2 t_0/a^2}. \tag{B3b}$$

Again we transform according to

$$v(r,t^*) = rc(r,t^*) \tag{B4}$$

to obtain the initial and boundary-value problem

$$\frac{\partial v}{\partial t^*} = D_F \frac{\partial^2 v}{\partial r^2}; \quad v(0,t^*) = 0, \quad \left.\frac{\partial v(r,t^*)}{\partial r}\right|_{r=a} = \frac{1}{a}v(a,t^*), \quad v(r,0) = rf(r). \tag{B5}$$

From the analysis in Appendix A we know that the solution is given by

$$v(r,t^*) = \sum_0^\infty C_n\phi_n(r)e^{-D_F\alpha_n^2 t^*}, \quad \beta_n = \tan\beta_n, \quad \beta_n = a\alpha_n. \tag{B6a}$$

where

$$\phi_0(r) = r, \quad \phi_n(r) = \sin(\alpha_n r) \tag{B6b}$$

We now determine the coefficients C_n. The first coefficient C_0 is given by

$$C_0 = \frac{\int_0^a \phi_0(r) r f(r)\mathrm{d}r}{\int_0^a \phi_0^2(r)} = \frac{3J_0t_0}{a} \tag{B7}$$

and we now must calculate

$$\frac{a}{2}\sin^2(a\alpha_n)C_n = \int_0^a r\sin(\alpha_n r)f(r)\mathrm{d}r \equiv J \tag{B8a}$$

where

$$J = J_1 + J_2 - J_3 \tag{B8b}$$

and

$$J_1 = A\int_0^a r\sin(\alpha_n r)\mathrm{d}r = 0, \quad J_2 = B\int_0^a r^3\sin(\alpha_n r)\mathrm{d}r = \frac{2Ba^4\sin\beta_n}{\beta_n^2}. \tag{B8c}$$

For J_3 we have

$$J_3 = \sum_{k=1}^\infty P_k\int_0^\infty \sin(\alpha_k r)\sin(\alpha_n r)\mathrm{d}r = \frac{a}{2}P_n\sin^2\beta_n. \tag{B9}$$

Then one obtains $J = J_2 - J_3$ and the coefficients for $n \geq 1$ are given by

$$C_n = \frac{2}{a}\frac{J}{\beta_n^2\sin\beta_n} = \frac{2J_0a^2}{D_F}\frac{1}{\beta_n^2\sin\beta_n}\left(1 - e^{-D_F\beta_n^2 t_0/a^2}\right). \tag{B10}$$

Now we can compute the subsidiary solution

$$v(r,t^*) = C_0\phi_0(r) + \sum_{n=1}^\infty C_n\phi_n(r)e^{-D_F\alpha_n^2 t^*} \tag{B11}$$

and apply (B4) to obtain

$$c(r,t^*) = \frac{3J_0t_0}{a} + \frac{2aJ_0}{D}\sum_{n=1}^\infty \frac{1}{\beta_n^2\sin\beta_n}\left(1 - e^{-D\beta_n^2 t_0/a^2}\right) \times \frac{\sin(\beta_n r/a)}{r/a}e^{-D_F\beta_n^2 t^*/a^2}. \tag{B12}$$

In dimensionless form we have

$$\frac{c(R,\tau^*)}{aJ_0/D} - 3\tau_0 = \frac{2}{R}\sum_1^\infty \frac{\sin(\beta_n R)\left(1 - e^{-\beta_n^2\tau_0^*}\right)}{\beta_n^2\sin\beta_n}e^{-\beta_n^2\tau^*}. \tag{B13}$$

where $\tau^* = D_F t^*/a^2$.

One can also determine the time evolution of the surface concentration for this initial value by setting $R = 1$ in (B13) to obtain

$$\frac{c(1,\tau^*)}{aJ_0/D_F} - 3\tau_0 = 2\sum_1^\infty \frac{\left(1 - e^{-\beta_n^2\tau_0}\right)}{\beta_n^2}e^{-\beta_n^2\tau^*}. \tag{B14}$$

References

[1] D. Ahn, R. Raj, J. Power Sources 195 (2010) 3900–3906, http://dx.doi.org/10.1016/j.jpowsour.2009.12.116.
[2] C.J. Wen, B.A. Baukamp, R.A. Huggins, W. Weppner, J. Electrochem. Soc. 126 (12) (1979) 2258–2266.
[3] W. Weppner, R.A. Huggins, Annu. Rev. Mater. Sci. 8 (1978) 269–311.
[4] W. Weppner, R.A. Huggins, J. Electrochem. Soc. 124 (1977) 1569–1578.
[5] E. Markevich, M.D. Levi, D. Aurbach, J. Electroanal. Chem. 580 (2005) 231–237.
[6] L. Cai, R.E. White, J. Power Sources 217 (2012) 248–255.
[7] P.E. Sanchez-Jimenez, R. Raj, J. Am. Ceram. Soc. 93 (2010) 1127–1135, http://dx.doi.org/10.1111/j.1551-2916.2009.03539.x.
[8] D. Ahn, R. Raj, J. Power Sources 196 (2011) 2179–2186, http://dx.doi.org/10.1016/j.jpowsour.2010.09.086.
[9] N.A. Kashkedikar, J. Maier, Adv. Mater. 21 (2009) 2664–2680, http://dx.doi.org/10.1002/adma.200901079.
[10] P.H. Bottelberghs, G.H.J. Broers, Electrochim. Acta 21 (1976) 719–726.
[11] X. Hu, S. Stanton, L. Cai, R.E. White, J. Power Sources 218 (2012) 212–220.